Influence of the solute concentration on the anelasticity in Mg-Al alloys: a multiple-approach study.

Daria Drozdenko[1,2,*], Jan Čapek[1], Bjørn Clausen[3], Alexei Vinogradov[4,5], Kristián Máthis[1]

[1]*Faculty of Mathematics and Physics, Charles University, Ke Karlovu 5, 121 16 Prague, Czech Republic*

[2]*Magnesium Research Center, Kumamoto University, 2-39-1 Kurokami Chuo-ku Kumamoto, 860-8555 Japan*

[3]*Materials Science & Technology Division, Los Alamos National Laboratory, Los Alamos, NM 87544, USA*

[4]*Department of Industrial and Mechanical Engineering, Norwegian University of Science and Technology – NTNU, Trondheim 7491, Norway*

[5]*Institute of Advanced Technologies, Togliatti State University, Togliatti, 445020, Russia*

[*]*correspondence author: drozdenko@karlov.mff.cuni.cz*

Abstract

The anelastic mechanical response caused by complex twinning-detwinning processes interacting with dislocation slip in Mg and its alloys is ubiquitous for their deformation behavior. A rare blend of advanced *in-situ* techniques with different spatiotemporal resolutions, including the acoustic emission (AE) measurements, neutron diffraction, *in-situ* SEM and high-speed microscopic video imaging, enabled access to otherwise inaccessible fine microstructural details of the underlying deformation mechanisms during cyclic loading of Mg alloys. Specifically, the influence of the alloying content on the anelastic behavior was characterized by the combination of these techniques. The applicability, advantages, and disadvantages of different *in-situ* techniques to study the deformation mechanisms in Mg alloys are discussed.

Keywords: Mg-Al alloy; twinning-detwinning; neutron diffraction; acoustic emission; high-speed camera; *in-situ* SEM

1. Introduction

In the last decade, Magnesium (Mg) alloys increased their share in the weight saving and biomedical applications. The design of safe structural elements, regardless of anticipated application, requires intimate knowledge about the mechanical performance under various circumstances, including strain-path changes, aggressive environment or elevated temperatures. The low symmetry of the hexagonal lattice structure of Mg determines many key features of its deformation behavior. The limited number of the equivalent slip systems obstructs the fulfillment of the von Mises criterion of five independent slip systems required for homogeneous plastic flow. Therefore, deformation twinning is usually activated during plastic straining. Deformation twins are of polar nature, and thus, their activation depends on the sense of the loading in general, and also with respect to the texture of the material. Furthermore, when the reversed load is applied, detwinning can occur. The twinning-detwinning phenomenon was found to be the main contributor to the specific strain hysteresis observed during the loading-unloading process [1-3]. Such an anelastic behavior makes it challenging to define and reliably measure the elastic moduli, which are essential in virtually all engineering calculations for structural design. Besides, this anelastic response in the cyclic deformation of Mg alloys affect strongly their fatigue performance, which is often below expectations and requires microstructural-based understanding and improvement.

The twinning – detwinning process has been studied in detail in numerous works. Proust et al. [4] proposed a theoretical model based on the viscoplastic self-consistent (VPSC) scheme describing the twinning behavior during the strain path change. Experimentally, acoustic emission (AE) and electron backscatter diffraction (EBSD) methods were used to follow the detwinning behavior during a single tension-compression cycle [5-7]. The hysteresis loops during loading-unloading were comprehensively studied by neutron diffraction (ND) [2, 8], where the detwinning process was evidenced by the re-growth of particular diffraction peaks. Besides, several modern techniques for *in-situ* microstructure observations, such the direct imaging during loading inside the chamber of the scanning electron microscope (SEM) or the high-speed video recording have emerged recently to provide the real-time information about microstructural changes with different temporal resolutions [9, 10].

The influence of the solute concentration on detwinning was investigated in several papers by Cáceres et al. [1] and recently by Cui et al. [11]. In binary Mg-Zn binary alloys, it

was found that the anelastic strain decreases with the increasing Zn content [1]. In Mg-Al alloys, this dependence was found to be less straightforward since the maximum anelastic strain for Mg-9 at.% Al alloy was doubled of that for Mg-0.5 at.% Al or Mg-2 at.% Al alloys. To date, there is no consensus on how the twinned volume and the number of twin boundary density are related to the anelastic strain. The relation of the strain to the twinned volume was studied by diffraction [12] and microscopy methods [11, 13]. Nagarajan [13], as well as Li and Enoki [14], investigated the role of the number of nucleated twins. However, a comprehensive study, in which both parameters are equally readily assessed, ideally a single experiment, is still missing in the literature.

Thus, the prime novelty of the present work consists in application of a blend of complementary experimental methods – the neutron diffraction (ND), acoustic emission (AE), and *in-situ* imaging by both high-speed camera and SEM - providing a statistically relevant dataset (i.e. investigating large sample volumes) for the investigation of anelasticity in Mg-Al binary alloys. The local *in-situ* SEM and rapid video observations were used for visual verification of the ND and AE results. Altogether, the above-mentioned techniques provide comprehensive information for multiscale analysis of the twinning process in fine temporal and spatial details during loading-unloading cycles. As has been shown in our recent works [15-17], the combination of AE technique and diffraction method with the support from *post-mortem* microstructure investigations offers consistent data regarding the number of nucleated twins and the overall twinned volume. Using the adaptive sequential *k*-means (ASK) cluster analysis for AE data proposed in [18] enabled characterization of the dynamics of deformation mechanisms with millisecond time resolution. Concurrently, the results of *in-situ* microstructure imaging provided evidence of activation or transition between different deformation mechanisms: dislocation slip, twin nucleation, and growth (including propagation and thickening), detwinning, during cyclic loading.

2. Experimental

Randomly textured pure Mg, binary Mg-2 wt.% Al and Mg-9 wt.% Al (hereafter, pure Mg, Mg2Al, and Mg9Al) were used. The specimens were solution heat-treated at 418 °C for 24 hours before the experiments. The grain sizes were (120 ± 10) μm for pure Mg and Mg9Al and (100 ± 15) μm for Mg2Al alloys. During casting of pure Mg, 1 wt.% Zr was added to the melt as a grain refiner. The Zr atoms can segregate in the grain interiors in form of halo

structures or at grain boundaries [19]. However, as it was shown in our previous works [15,16], their influence on the twinning process is negligible.

The detwinning phenomenon was studied by means of repeated loading-unloading cycle: the specimens were deformed in compression to predefined strains set at 0.05%, 0.1%, 0.5%, 1%, 2%, 3%, and 6%. After reaching a particular strain value, the sample was unloaded to zero stress and then re-loaded up to the next strain value. Threaded cylindrical specimens with a gauge diameter of 9 mm and a gauge length of 20 mm were used for the mechanical testing.

The *in-situ* ND measurements during cyclic loading were carried out at the SMARTS engineering instrument in the Lujan Neutron Scattering Center [20]. The longitudinal axis of the sample was tilted from the incident neutron beam by 45°. The two detector banks were positioned at ±90° to the incident beam in order to record the diffraction pattern in both longitudinal and normal directions (both defined with respect to the loading direction). Details of the experimental setup are provided in [17]. In order to collect representative ND data, the tests were interrupted at predefined strain levels for approximately 15 min. Loading was carried out using a horizontal 250 kN capacity load frame at the nominal strain rate of 1×10^{-3} s^{-1} under strain control. All deformation tests were performed at room temperature.

The AE response was recorded using the Mistras PCI-2 acquisition board. A broadband WD-type AE sensor (Mistras corporation) was mounted outside of the gauge part of the specimen using vacuum grease and an elastic band. The AE signal was amplified by 60 dB in the frequency range of 100 – 1200 kHz. The AE response was monitored in two modes of recording:

i) Hit-based recording was performed concurrently with ND measurements. In this recording mode, the signal is parametrized by setting a threshold level (set slightly above the level of background noise) and hit definition time (HDT). The recording of a single AE event starts, when the signal cross first the threshold, and terminates, when it remains below threshold for HDT. The threshold level and the HDT were set at 30 dB and 800 µs, respectively.

ii) Data streaming refers to the method of continuous recording of the raw signal in a threshold-less mode during the same loading-unloading testing procedure as above. In this case, the test was carried out continuously without holding times for collecting ND data. Data from this type of recording was used for the ASK analysis afterward. The detailed description of the ASK algorithm and methodology of the analysis can be found in [17, 18].

In-situ observations of the microstructure evolution were performed during loading by means of a high-speed camera and SEM. For video recording, a custom-made setup based on the Photron FASTCAM SA3 high-speed video camera triggered by the AE signal recorded by the PCI-II board was used as described in [21]. The polished specimen was tested at the crosshead velocity of 2 mm/s. Video recording was performed at different rates from 30 to 1000 fps.

For a better spatial resolution, *in-situ* observations were also performed in the chamber of the SEM Zeiss Crossbeam Auriga. The specimens were first ground and polished using a diamond paste down to ¼ μm particle size. In the following step, electrolytic polishing using a Struers AC2 electrolyte was performed at 18 V and -40°C. Using the deformation stage MTEST Quattro (Materials Testing system ADMET), installed inside the SEM chamber, the specimens were gradually loaded up to 75, 90, 115, 130, 180, 220 and 260 MPa (i.e. up to the same levels as those used during testing with concurrent AE and ND measurements). Upon reaching each desired stress value, the specimens were unloaded down to the minimum level of 2 MPa. Complete unloading was not possible for technical reasons regulating the sample mounting inside the SEM chamber. In each pre-defined stress levels, both secondary electrons (SE) and backscatter electrons (BSE) images were taken, and, afterward, the EBSD maps were acquired to reveal the crystallographic orientation of grains and twins, respectively.

3. Results

3.1. Anelastic behavior of Mg-Al alloys

Measured stress-strain curves are presented in Fig. 1. All the alloys exhibit the pronounced anelastic behavior during unloading. Two regions of the mechanical response can be distinguished: 1) the elastic and microplastic deformation up to the yield point, and 2) the macroplastic deformation above the yield point. Magnified views of the deformation curves up to the 0.5% strain range are shown in Fig. 1b-d for different alloys showing the remarkably different mechanical response to loading-unloading cycle. The microplastic behavior can be noticed in pure Mg at the very low stress (~2 MPa indicated by the horizontal arrow in Fig. 1b, while the macroscopic yielding occurs at around 25 MPa (the vertical arrow). The unloading-reloading curve forms a hysteresis loop already in the microplastic region. In the Mg2Al sample, the microplastic deformation becomes appreciable at 25 MPa, while the macroplastic flow begins at around 50 MPa, respectively. As opposes to pure Mg, the

hysteresis loop in the Mg2Al sample appears only above the macroscopic yield point, Fig. 1c. In the Mg9Al sample, the microplasticity is completely absent and the macroplasticity starts at about 50 MPa, Fig. 1d.

The anelastic strain range ($\Delta\varepsilon$) is defined in Fig. 1d as the width of the hysteresis loop on the true stress- true plastic strain curve. The strain dependence of the anelastic strain is plotted in Fig. 2. For the strains below 0.5% of the plastic strain, the anelasticity for pure Mg is larger than that for the Mg2Al sample. Above this limit ,the Mg9Al sample demonstrates the greatest anelasticity within the investigated materials. The maximum anelasticity is seen at around 2% of plastic strain for all alloys. These results are in good agreement with the findings reported in [13].

The results reported in [1, 11] indicate that the relation exists between the twinning-detwinning phenomenon and the anelasticity. The analysis of ND data allows for evaluating the twinned volume fraction (TVF) along the deformation path is shown in Fig. 3[1] (the details of the TVF calculation are presented in [22]). The linear dependence of TVF on the plastic strain is evident in the strain range examined. Furthermore, during unloading, the TVF value reduces. However, it still follows essentially the same linear dependence. The largest change in TVF during unloading is observed for the Mg9Al alloy, Fig. 4. This means that detwinning is more pronounced in this alloy compared to other investigated materials.

The twinning process consists of three main stages: nucleation (appearance of the twin nucleus), propagation (length-wise extension) and growth (thickness-wise extension). The diffraction methods can generally characterize the change of the twinned volume, which is associated primarily with the growth stage. However, these methods yield virtually no information about the number of nucleated twins, which can be nicely monitored by the AE method, as it is particularly sensitive to twin nucleation and propagation [23]. This means that the AE response during straining is proportional to the number of the nucleated twins. Consequently, the AE testing can provide conclusive information, whether the hysteresis loop shape is controlled by the motion of the pre-existing twin boundaries, or the nucleation (and propagation) of new twins also takes place and contributes to the anelastic effect.

At first, the AE results measured in the hit-based mode provide the following information. Owing to the heat treatment applied to the samples before mechanical testing, there are no twins presented in the initial microstructure. Therefore, the initial loading is

[1] The data are shifted by 0.5% of plastic strain for visibility

expected to be accompanied by twin nucleation. In contrast, on the reloading stage of the hysteresis loop, both the growth of twins nucleated in the previous cycle, as well as the nucleation of new twins can occur.

The obtained AE events can be divided into three different groups according to the time of their appearance along the loading path, Fig. 5:

- AE during ND spectrum measurement, when relaxation of samples takes place (black squares);
- AE during unloading and reloading until the previous maximal stress is reached (green triangles);
- AE after reaching the previous maximal stress level (red circles).

It is obvious that the AE response significantly depends on the Al content. There is no AE during unloading of pure Mg samples. Upon reloading, the AE behavior follows the Kaiser-effect [24], this is AE reappears only when the applied stress exceeds the peak value reached at the previous loading cycle. Some appreciable AE has been detected during unloading of the Mg2Al samples and the Kaiser-effect is almost obeyed (except some sporadic events seen on the uploading part of the hysteresis loops) during the reloading. In contrast, strong AE has detected already during the unloading and reloading in the Mg9Al alloy and the Kaiser effect is no longer observed.

It is a well known fact that twinning is an important contributor to the overall AE signal. However, owing to several concurrently active AE mechanisms in Mg alloys – dislocation slip and twinning, the hit-based AE recording is not suitable for categorization of the particular AE events [23]. To elucidate the relative contribution of each emitting source to the resultant AE and to identify the dominant mechanism during different stages of the unloading-reloading loop, the non-supervised ASK cluster analysis was applied to the AE data streams. Since the results for pure Mg and Mg2Al alloy are almost identical, only the pure Mg and Mg9Al samples are presented below.

The details of the ASK clustering algorithm in application to the deformation behavior of Mg alloys have been discussed in our previous papers [17, 25]. The continuously recorded data were sectioned into consecutive individual realizations (“frames”) containing 2048 samples. The frames were then classified based on the similarity/dissimilarity of their power spectral density (PSD) functions $G(f)$ calculated by the Welch method [18]: the frames with the similar normalized PSDs were grouped into a set of clusters with minimized intra-cluster

distances and maximized inter-cluster distances. The number of clusters is not pre-set, but is data-driven and is suggested automatically by the ASK algorithm. The Kullback-Leibler divergence [26] (in its symmetrical version) has been used as a measure of similarity of the shapes of normalized PSDs. Application of the non-supervised ASK procedure shows that all realizations (frames) fall naturally into three major categories differed by their PSD shapes as shown in Fig. 6a representing the centroids of the AE clusters. Based on the time of appearance and mutual distributions of physical parameters (amplitude, energy, frequency range) of the cluster elements (see, for example, Fig. 6b), a dominant AE source mechanism is associated with each cluster. Since the continuous AE recording was launched before starting the deformation, the first cluster, having low energy and broad frequency range is naturally attributed to the background noise, Fig. 6b. The cluster related to dislocation slip exhibits low- to medium energies. It is reasonably low-frequency and has a characteristic shape in the *Energy-Median Frequency* coordinates. The signals from this cluster emerge at low stresses immediately after the beginning of loading, which is in good agreement with the low critical resolved shear stress of basal slip. The high amplitude and power signals from the cluster created by twinning events fell into a narrow frequency range in the high-frequency domain that corresponds to a large reoriented volume and fast twin propagation.

In the pure Mg sample, the dominancy of a particular mechanism (twinning or slip) in the AE spectrum depends on the deformation stage. The noise is recognized at low stresses, both at the onset of loading and at the time of the strain path reversal. The dislocation slip dominates the deformation behavior during the initial state of unloading and during entire reloading. Twinning is the most pronounced mechanism operating above the maximum stress reached during the previous loading cycle (i.e. during the monotonic compressive loading session), Fig. 7a. In contrast, in the Mg9Al sample, the twinning represents the major deformation mechanism over the entire test, independently of the stage of the loading cycle, Fig. 7b.

Such behavior indicates that in the Mg9Al alloy the twin propagation contributes to the AE signal also during the unloading-reloading loop.

To validate the results of the indirect AE clustering, the direct high-speed imaging of the microstructure evolution was used. The microstructures of pure Mg sample loaded up to 50 MPa (Fig. 8a) and unloaded (Fig. 8b) look similar. A closer view (see the crossover of highlighted twinned areas in the middle of Fig. 8) shows that only a slight shrinking of the twin occurs upon unloading (red area – at 50 MPa, green area – at 0 MPa). In contrast, in the

Mg9Al alloy significant shrinking or the complete disappearance of twins is observed after unloading from 125 MPa, see Fig. 9.

3.2. Microstructure evolution in the Mg9Al alloy with high anelasticity during cyclic loading

The deformation processes accompanying anelasticity are most pronounced in the Mg9Al sample. Therefore, this material was subjected to additional *in-situ* SEM observations during the same cyclic loading procedure as above. The progression of main deformation mechanisms, which are active during cyclic loading, can be seen in Fig. 10, where the snapshots of the deformed surface are presented at different applied loads.

Traces of basal dislocations emerging at the free surface become visible already after the first cycle of loading up to 75 MPa (highlighted by red lines in Fig. 10a). With the increasing applied load, more slip lines are observed at the surface, Fig. 10b. At the next round of the cyclic loading up to 115 MPa, tiny twins show up on the surface (marked by orange arrows in Fig. 10c), which then become thicker with increasing stress, Fig. 10d,e. Concurrently with the increasing twinning activity, the amount of dislocation slip traces increases at each compression step of cyclic loading. Finally, the highly deformed microstructure can be seen after cyclic loading up to 220 MPa, Fig. 10f. It is noteworthy that high-speed camera reveals basal traces later if compared to SEM images. The basal slip lines appear on the video images in the same shot with the first twins while the SEM images reveal the first basal slip lines at the lower stress, and, then as deformation proceeds, the twins appear in the field of view. Thus, SEM imaging is more powerful for observing the dislocation slip evolution due to its higher resolution. However, the high acquisition rate of optical video imaging enables monitoring of rapid twin propagation and growth [10], which is not possible with SEM imaging.

SEM-SE observations revealing the detwinning process during unloading are represented in Fig. 11. Complementary, the results of the Schmid factor (SF) analysis for twin nucleation and basal slip are shown in Fig. 12. During cyclic loading, the twins showed up in the microstructure first time after reaching 115 MPa, Fig. 11. Then, during unloading from 115 MPa the complete disappearance of the thin tip of the twin (i.e. shortening the twin length) together with the slight shrinkage of the twin's thickness is observed (these changes are highlighted by red arrows in Fig. 11). During the next reloading up to 130 MPa several new twins nucleate (for example, the one marked by the yellow arrow in Grain 1 in Fig. 11c).

However, they completely disappear during the subsequent unloading (see Fig. 11d). Moreover, it should be noticed that, in contrast to the just discussed detwinning by shortening of the twin length, detwinning in the latter case proceeds by thickness reduction and leftover a twin embryo close to the grain boundaries (pointed out by the red arrows in the central grain in Fig. 11d). The SF_{tw} value for this twin is quite high, i.e. of 0.32.

The majority of twins nucleate in grains with high SF for twinning: original lattice orientation (O.) and nucleated twins (tw.) are marked in Fig. 11 for some selected grains. In grain 1, Fig. 11e-f, twins originate at the grain boundary connected to Grain 2 with multiple twinning inside. No twins were observed in Grain 3. Multiple twinning in grain 1 can be explained by high SF_{tw} (0.47), see Fig. 12. Despite low SF_{tw} in Grain 2, twins are nucleated and grow there. The twinning activity significantly increases during further reloading up to 180 MPa, and many newly created (quite thick) twins can be observed, Fig. 11e. It should be noted that, when other twins nucleated in the grain (e.g. in Grain 1), the existing twins become less active and their length-wise growth does not occur, i.e. the terminal length for this twin is achieved. Upon further reloading up to 220 MPa, primarily twin thickening takes place, Fig. 11g and the slight twin shrinkage is observed during unloading similarly to the previous cases, Fig. 11h.

Numerous visible traces of basal slip correlate well with the high SF values for basal slip, Fig. 12. Naturally, SF_{basal} for basal slip in the lattice reoriented by twinning is higher comparing to that in the original lattice. An example of the visible traces of basal slip can be easily found in the magnified image of the Grain 1, Fig. 13. It is evident that the basal slip activates immediately inside the newly created twin. Clear traces of basal dislocation slip are well seen after the deformation test involving the loading stage up to 220 MPa followed by unloading, Fig. 13b). However, the dislocation slip traces in the twinned regions were observed even earlier, at lower stresses, i.e. shortly after nucleation of this twin under loading up to 130 MPa, Fig. 13a.

4. Discussion

The strain dependence of the anelasticity on the solute content can be divided into two domains. At low strains (<0.1%), the $\Delta\varepsilon$ value is the largest for pure Mg and it decreases with the increase in the Al content, Fig. 2. The opposite trend is observed at high strains, where the largest anelasticity is seen for the Mg9Al alloy.

From Fig. 2 and 4 it can be seen that the change of TVFs during unloading is directly proportional to $\Delta\varepsilon$, Fig. 14. All data fall on the same master straight line with the slope seemingly independent on the chemical composition. This means that the alloying influences the anelasticity through controlling the mobility of the twin boundaries.

As it has been shown by Ghazisaeidi et al. [27] and Cui et al. [11], the presence of solute atoms hinders the movement of twin dislocations and increases the friction stress for twin boundary motion. In the case of pure Mg, owing to the lack of the solute atoms in the grain interior, coherent twin boundaries have been observed [11]. The mobility of these boundaries is quite high. The stress necessary for the twin growth can be estimated from the hysteresis loop since during the reloading stage the onset of plastic deformation is controlled mainly by the twin growth. Thus, the stress value, at which the reloading curve deviates from the elasticity corresponds approximately to the twin growth stress. It is less than 2 MPa for pure Mg (being similar to the stress required for twin nucleation). Thus, in pure Mg, the twins can reach a critical aspect ratio at relatively low stress, and thus the stresses at the sides of the twins completely relax [28]. Consequently, the driving force for detwinning becomes almost zero. In summary, in pure Mg, the twinning-detwinning process prevails only at loops formed at low applied stresses, where the largest anelasticity is observed. In the case of binary alloys, several effects have to be taken into the account. For example, for the Mg2Al alloys, softening of the prismatic planes has been reported [1, 13, 29], which makes the activation of the prismatic slip more favorable than twinning at low stresses. At the same time, the solutes shift the CRSS for twin nucleation towards higher values [29]. Finally, as a consequence of the interaction of the solute atoms with the twin boundaries, the serrated twin boundaries with low mobility can form [11]. The stress necessary for twin growth in the Mg2Al alloy is estimated to be of 20 MPa, which is significantly lower than the value required for twin nucleation (of 50 MPa). In the case of the Mg9Al sample, the full development of twinning takes place at the macroscopic yield point, and the stress values necessary for twin nucleation and growth appear to be comparable.

It is worth to note that the appearance of other twins in the same grain leads to the redistribution of internal stress, which can also lead to the relaxation of lateral twin stresses and to termination of the twin growth (cf. Fig. 11e) [28]. As in compression, the number of nucleated twins (and twin variants) per grain is smaller in the grains with higher SF_{tw} [30, 31]. Consequently, the twins can easily grow. In contrast, in tension, 4 to 6 variants of twins can be observed within a single grain with the high SF_{tw} values. This leads to smaller twin

dimensions, easier detwinning, and larger anelasticity. It can be thus suggested that the extent of the anelastic behavior in randomly textured materials can be different for tension and compression, respectively, as it was indicated by Mann [1] and Nagarajan [13]. However, this assumption needs further experimental verification.

An important outcome of the present work is that the results of all independent *in-situ* methods: the high-speed microscopic video recordings, *in-situ* SEM and AE testing – appear in excellent agreement with the ND results and theoretical assumptions.

For pure Mg, the non-supervised ASK AE cluster analysis shows that at low stresses (< 25 MPa) the dislocation slip and twinning are mutually active during both unloading and reloading. With the increasing stress, a phase shift between the time appearance of the increment of slip and twinning clusters can be observed. During unloading, the sample is quiet (only the background noise can be detected). During reloading, the dislocation slip is active, whereas the twin cluster starts to increase only after reaching the maximum stress from the previous cycle. This is in agreement with the assumption that at higher stresses the twins only slightly shrink, which is not accompanied by detectable AE. During the reloading, they can start to grow again, since the required stress is low, and the AE signals are originated from local microplastic slip events. New, audible twins nucleate only after reaching the maximum stress from the previous cycle.

In the case of the Mg9Al alloy, AE is detected during both unloading and reloading. Fig. 9 confirms unambiguously, that complete detwinning occurs in the Mg9Al alloy. Therefore, during reloading, new twins are nucleated and are accompanied by the strong AE transients. It is worth noting that the ASK analysis does not exclude the concurrent activity of other deformation mechanisms. Rather it determines the dominant source of AE in the given time interval. As it is obvious from SEM imaging in Figs. 10-13, that the basal slip also takes place both in original microstructure and reoriented lattice of a newly created twin.

Nevertheless, the detectable AE during unloading deserves a more detailed consideration, since it is rarely observed [14].

The twinning – detwinning process and its correlation to AE response are schematically outlined in Fig. 15. Twinning can be described as a multistage process comprising of fast twin nucleation and length-wise propagation generating detectable AE, followed by slow twin thickening that is not detectable by AE. During unloading, the mechanism mediating the overall mechanical response is twin shrinking, which is mirroring the twin thickening and is not detectable by AE as has been reported previously [32]. However, in the Mg9Al alloy,

several additional processes, which are intimately related to the twinning-detwinning mechanisms, have been observed. Specifically: (i) the thick twins become slightly thinner, (ii) some of the thin twins reach a critical width, which leads to their virtually complete disappearance at zero stress. , Fig. 11c-d, or (iii) thin tip of the twin disappears (i.e. shortening of the twin length occurs), Fig. 11a-b. Last two processes are supposed to produce the detectable AE signal due to the high speed of twin length reduction (c.f. Fig. 10a-b; c-d) comparable to the speed of twin propagation. It was shown in [5] that the rapid velocity of twin propagation is a decisive factor for AE detectability. Therefore, the "fast" collapse of thin twins during unloading in the Mg9Al alloy generates the detectable AE transient, while the "slow", incomplete shrinking in the Mg2Al alloy and pure Mg does not produce the measurable AE signal. In Fig. 11c-d, significant thickness shrinkage and therefore disappearance of the twin. However, the twin embryo still remains close to grain boundaries (detailed view in Fig. 11d), can be also counted as a fast reduction of the twin length. In this case, the observation field of view limits us to the 2D surface fragment, while the twin length reduction can proceed in the direction perpendicular to the image plane.

5. Conclusion

The complex twinning-detwinning processes resulting in the pronounced anelasticity of Mg and its alloys were investigated by a combination of several *in-situ* techniques with different temporal and spatial resolutions. These techniques included the continuous acoustic emission measurements, neutron diffraction, *in-situ* scanning electron microscopy, and high-speed video imaging during cyclic loading of Mg and its alloys. The following conclusions can be drawn:

1. The anelasticity effect in Mg alloys is closely connected to the twinning-detwinning process, as the change in the twinned volume is directly proportional to the anelasticity for all investigated alloys. Above 0.5% of plastic strain, the anelasticity is more pronounced in the highly alloyed sample (Mg9Al) than that in pure Mg and low alloyed sample (Mg2Al). Below this limit, pure Mg exhibits the highest anelasticity.
2. The aluminum content increases the stress necessary for the twin nucleation and growth. Therefore, only thin twins form in the Mg9Al alloy, which can completely detwin upon unloading. In contrast, thick twins develop even at low applied stresses in pure Mg and Mg2Al alloys, which partially shrink, but do not completely disappear during unloading.

3. The *in-situ* scanning electron microscopy and high-speed imaging revealed the microstructural processes underlying the acoustic emission behavior on different stages of the loading-unloading hysteresis loops in the Mg9Al alloy: during unloading, the reduction of the twin length takes place, which is a high-speed process accompanied by detectable acoustic emission transients. On the reloading stage, the nucleation of new twins contributes to detectable acoustic emission in the Mg9Al alloy. As opposed to this, in pure Mg and Mg2Al alloy, only the slow movement of existing twin boundaries occurs, and this process does not generate detectable acoustic emission.

4. *In-situ* scanning electron microscopy imaging is the most powerful method for tracking the dislocation slip activity requiring high spatial resolution of the surface topology. High-speed microscopic video imaging is particularly beneficial for the estimation of the speed of twin nucleation, propagation, and growth. However, the resolution achieved by SEM imaging offers more opportunities for observing the microstructural details of underlying processes, such as twin thickening – thinning, dislocation slip and its interaction.

Acknowledgments

The authors are grateful for the financial support of the Czech Science Foundation under the contract 18-07140S. AV acknowledges the support from the Ministry of Education and Science of RF through the State Assignment according to the contract No. 11.5281.2017/8.9.

This work has benefited from the use of the Lujan Neutron Scattering Center at LANSCE, funded by the US Department of Energy's Office of Basic Energy Sciences. Los Alamos National Laboratory is operated by Los Alamos National Security LLC under US DOE Contract DE-AC52-06NA25396.

The authors are also highly grateful to Petr Harcuba for help during *in-situ* SEM measurements.

References

[1] G.E. Mann, T. Sumitomo, C.H. Cáceres, J.R. Griffiths, Reversible plastic strain during cyclic loading-unloading of Mg and Mg-Zn alloys, Mater. Sci. Eng., A., 456 (2007) 138-146. https://doi.org/10.1016/j.msea.2006.11.160.

[2] M.A. Gharghouri, G.C. Weatherly, J.D. Embury, J. Root, Study of the mechanical properties of Mg-7.7at.% Al by in-situ neutron diffraction, Philos. Mag. A, 79 (1999) 1671-1695. https://doi.org/10.1080/01418619908210386.

[3] H.Q. Ang, T.B. Abbott, S. Zhu, M.A. Easton, Anelasticity of die-cast magnesium-aluminium based alloys under different strain rates, 707 (2017) 101-109. https://doi.org/10.1016/j.msea.2017.09.012.

[4] G. Proust, C.N. Tome, A. Jain, S.R. Agnew, Modeling the effect of twinning and detwinning during strain-path changes of magnesium alloy AZ31, Int. J. Plasticity, 25 (2009) 861-880. https://doi.org/10.1016/j.ijplas.2008.05.005.

[5] A. Vinogradov, E. Vasilev, M. Linderov, D. Merson, In situ observations of the kinetics of twinning-detwinning and dislocation slip in magnesium, Mater. Sci. Eng., A., 676 (2016) 351-360. https://doi.org/10.1016/j.msea.2016.09.004.

[6] X.Y. Lou, M. Li, R.K. Boger, S.R. Agnew, R.H. Wagoner, Hardening evolution of AZ31B Mg sheet, Int. J. Plasticity, 23 (2007) 44-86. https://doi.org/10.1016/j.ijplas.2006.03.005.

[7] D. Drozdenko, J. Bohlen, S. Yi, P. Minárik, F. Chmelík, P. Dobroň, Investigating a twinning-detwinning process in wrought Mg alloys by the acoustic emission technique, Acta Mater., 110 (2016) 103-113. https://doi.org/10.1016/j.actamat.2016.03.013.

[8] O. Muransky, M.R. Barnett, D.G. Carr, S. Vogel, E.C. Oliver, Combined in situ neutron diffraction and acoustic emission of twin nucleation & twin growth in extruded ZM20 Mg alloy, Mater. Sci. Forum, 652 (2010) 149-154. https://doi.org/10.4028/www.scientific.net/MSF.652.149.

[9] C.M. Cepeda-Jimenez, J.M. Molina-Aldareguia, M.T. Perez-Prado, EBSD-Assisted Slip Trace Analysis During In Situ SEM Mechanical Testing: Application to Unravel Grain Size Effects on Plasticity of Pure Mg Polycrystals, Jom-Us, 68 (2016) 116-126. https://doi.org/10.1007/s11837-015-1521-6.

[10] A. Vinogradov, E. Vasilev, M. Seleznev, K. Máthis, D. Orlov, D. Merson, On the limits of acoustic emission detectability for twinning, Mater. Lett., 183 (2016) 417-419. https://doi.org/10.1016/j.matlet.2016.07.063.

[11] Y.J. Cui, Y.P. Li, Z.C. Wang, X. Ding, Y. Koizumi, H.K. Bian, L.Y. Lin, A. Chiba, Impact of solute elements on detwinning in magnesium and its alloys, Int. J. Plasticity, 91 (2017) 134-159. https://doi.org/10.1016/j.ijplas.2016.09.014.

[12] L. Wu, S.R. Agnew, D.W. Brown, G.M. Stoica, B. Clausen, A. Jain, D.E. Fielden, P.K. Liaw, Internal stress relaxation and load redistribution during the twinning-detwinning-dominated cyclic deformation of a wrought magnesium alloy, ZK60A, Acta Mater., 56 (2008) 3699-3707. https://doi.org/10.1016/j.actamat.2008.04.006.

[13] D. Nagarajan, X. Ren, C.H. Caceres, Anelastic behavior of Mg-Al and Mg-Zn solid solutions, Mater. Sci. Eng., A., 696 (2017) 387-392. https://doi.org/10.1016/j.msea.2017.04.069.

[14] Y.P. Li, M. Enoki, Twinning behavior of pure magnesium quantitatively investigated by acoustic emission, Mater. Sci. Eng., A., 536 (2012) 8-13. https://doi.org/10.1016/j.msea.2011.10.010.

[15] G. Garcés, K. Máthis, J. Medina, K. Horváth, D. Drozdenko, E. Oñorbe, P. Dobroň, P. Pérez, M. Klaus, P. Adeva, Combination of in-situ diffraction experiments and acoustic emission testing to understand the compression behavior of Mg-Y-Zn alloys containing LPSO phase under different loading conditions, Int. J. Plasticity, 106 (2018) 107-128. https://doi.org/10.1016/j.ijplas.2018.03.004.

[16] J. Čapek, K. Máthis, T. Krajňák, The use of acoustic emission and Neutron diffraction to reveal the active deformation mechanisms in polycrystalline magnesium and comparison to theoretical modeling, in: Magnesium Technology, 2016, pp. 213-216.

[17] K. Máthis, G. Csiszár, J. Čapek, J. Gubicza, B. Clausen, P. Lukáš, A. Vinogradov, S.R. Agnew, Effect of the loading mode on the evolution of the deformation mechanisms in randomly textured magnesium polycrystals - Comparison of experimental and modeling results, Int. J. Plasticity, 72 (2015) 127-150. https://doi.org/10.1016/j.ijplas.2015.05.009.

[18] E. Pomponi, A. Vinogradov, A real-time approach to acoustic emission clustering, Mech. Syst. Signal Process, 40 (2013) 791-804. http://dx.doi.org/10.1016/j.ymssp.2013.03.017.

[19] M. Qian, D.H. StJohn, M.T. Frost, Characteristic zirconium-rich coring structures in Mg–Zr alloys, 46 (2002) 649-654. https://doi.org/10.1016/S1359-6462(02)00046-5.

[20] M.A.M. Bourke, D.C. Dunand, E. Ustundag, SMARTS - a spectrometer for strain measurement in engineering materials, Appl. Phys. A, 74 (2002) S1707-S1709. https://doi.org/10.1007/s003390201747.

[21] M. Seleznev, A. Vinogradov, Note: High-speed optical imaging powered by acoustic emission triggering, Rev. Sci. Instrum., 85 (2014) 076103. https://doi.org/10.1063/1.4890436.
[22] B. Clausen, C.N. Tome, D.W. Brown, S.R. Agnew, Reorientation and stress relaxation due to twinning: Modeling and experimental characterization for Mg, Acta Mater., 56 (2008) 2456-2468. https://doi.org/10.1016/j.actamat.2008.01.057.
[23] A. Vinogradov, K. Máthis, Acoustic emission as a tool for exploring deformation mechanisms in magnesium and its alloys in situ, Jom-Us, 68 (2016) 3057-3062. https://doi.org/10.1007/s11837-016-1966-2.
[24] J. Kaiser, Untersuchung über das Auftreten von Geräuschen beim Zugversuch, in, TU München, 1950.
[25] K. Horváth, D. Drozdenko, K. Máthis, J. Bohlen, P. Dobroň, Deformation behavior and acoustic emission response on uniaxial compression of extruded rectangular profile of Mg-Zn-Zr alloy, J. Alloy Compd., 680 (2016) 623-632. https://doi.org/10.1016/j.jallcom.2016.03.310.
[26] S. A Kullback, R.A. A Leibler, On Information and Sufficiency, Ann. Math. Stat., 22 (1951) 79-86. https://doi.org/10.1214/aoms/1177729694.
[27] M. Ghazisaeidi, L.G. Hector, W.A. Curtin, Solute strengthening of twinning dislocations in Mg alloys, Acta Mater., 80 (2014) 278-287. https://doi.org/10.1016/j.actamat.2014.07.045.
[28] F. Siska, L. Stratil, J. Cizek, A. Ghaderi, M. Barnett, Numerical analysis of twin thickening process in magnesium alloys, Acta Mater., 124 (2017) 9-16. https://doi.org/10.1016/j.msea.2011.10.010.
[29] K. Máthis, J. Čapek, B. Clausen, T. Krajňák, D. Nagarajan, Investigation of the dependence of deformation mechanisms on solute content in polycrystalline Mg-Al magnesium alloys by neutron diffraction and acoustic emission, J. Alloy Compd., 642 (2015) 185-191. https://doi.org/10.1016/j.jallcom.2015.03.258.
[30] J. Čapek, K. Máthis, B. Clausen, M. Barnett, Dependence of twinned volume fraction on loading mode and Schmid factor in randomly textured magnesium, Acta Mater., 130 (2017) 319-328. https://doi.org/10.1016/j.actamat.2017.03.017.
[31] I.J. Beyerlein, L. Capolungo, P.E. Marshall, R.J. McCabe, C.N. Tome, Statistical analyses of deformation twinning in magnesium, Philos. Mag., 90 (2010) 2161-2190. https://doi.org/10.1080/14786431003630835.

[32] D. Drozdenko, J. Bohlen, F. Chmelík, D. Letzig, P. Dobroň, The influence of rolling conditions in deformation behavior of magnesium alloy sheets, Acta Phys. Pol. A, 128 (2015) 795-800. https://doi.org/10.12693/APhysPolA.128.795.

List of figure captions

Fig. 1 Deformation curves during a repetitive loading-unloading cycle of Mg-Al alloys as a function of the composition (Fig. 1a). The onsets of the microplasticity and macroplasticity for the particular alloys (Fig. 1b-d) are indicated by the horizontal and vertical arrows, respectively. Fig. 1d indicates the definition of the anelastic strain.

Fig. 2 Dependence of the anelasticity on the plastic strain as a function of the aluminum content. The low strain values are zoomed in a log-log chart in the inserted graph.

Fig. 3 Evolution of the twinned volume fraction (TVF) during the repetitive loading and unloading of the samples. The full symbols indicate the TVF at loaded state, the empty symbols at unloaded state, respectively.

Fig. 4 Dependence of the twinned volume fraction (TVF) changes on the applied strain

Fig. 5 Acoustic emission events during the particular stages of the loading cycle (compressive loading – red circle; relaxation during diffraction pattern recording – black square; unloading – green triangle) for a) pure Mg, b) Mg2Al, c) Mg9Al

Fig. 6 a) Characteristic normalized power spectral density (PSD) functions and b) energy – mean frequency cross-plot for the acoustic emission clusters identified by the adaptive sequential *k*-means (ASK) analysis

Fig. 7 Evolution of the number of elements in the clusters assigned to particular acoustic emission source mechanisms for a) pure Mg and b) Mg9Al a as it given by adaptive sequential *k*-means (ASK) analysis.

Fig. 8 High-speed camera observation: microstructure of pure Mg after a) loading up to 50 MPa and b) unloading up to 0 MPa. Red color represents the twinned area at 50MPa, the green one that after the subsequent unloading. In the center chart the areas of highlighted twins on Fig. 8a and b are compared.

Fig. 9 High-speed camera observation: microstructure of the Mg9Al sample after a) loading up to 125 MPa and b) unloading back to 0 MPa. Shrinkage of twins is marked by arrows and complete detwinning - by circles. The black arrow at the bottom indicates the loading axis.

Fig. 10 *In-situ* SEM imaging: microstructure of the Mg9Al alloy after loading up to a) 75 MPa, b) 90 MPa, c) 115 MPa, d) 130 MPa, e) 180 MPa, f) 220 MPa, while each step of loading was followed by unloading up to 2 MPa. Red lines highlight traces of basal dislocation in grains, orange arrows – newly nucleated twins

Fig. 11 *In-situ* SEM imaging: microstructure of the Mg9Al sample after (re)loading and unloading at each step of cyclic loading. Newly created twins and twin growth are highlighted by the yellow arrows, while detwinning is pointed out by the red one. O. - origin lattice orientation of the grain; tw. - twin orientation

Fig. 12 Schmid factor calculation for the Mg9Al alloy: the values for basal slip are marked in green, the values for twins are marked in yellow

Fig. 13 *In-situ* SEM imaging: microstructure of the Mg9Al alloy after loading up to a) 130 MPa and b) 220 MPa and unloading up to 2 MPa. Traces of the dislocation lines correspond to basal slip

Fig. 14 Relation between the twinned volume fraction change during unloading and the anelastic strain for the particular specimens. Within the experimental error, all data follows a master straight line.

Fig. 15 Schematics of different stages of the twinning-detwinning process. Arrows indicate the direction of twin propagation: green color represents processes accompanied by detectable AE; red color corresponds to the processes which do not produce detectable AE

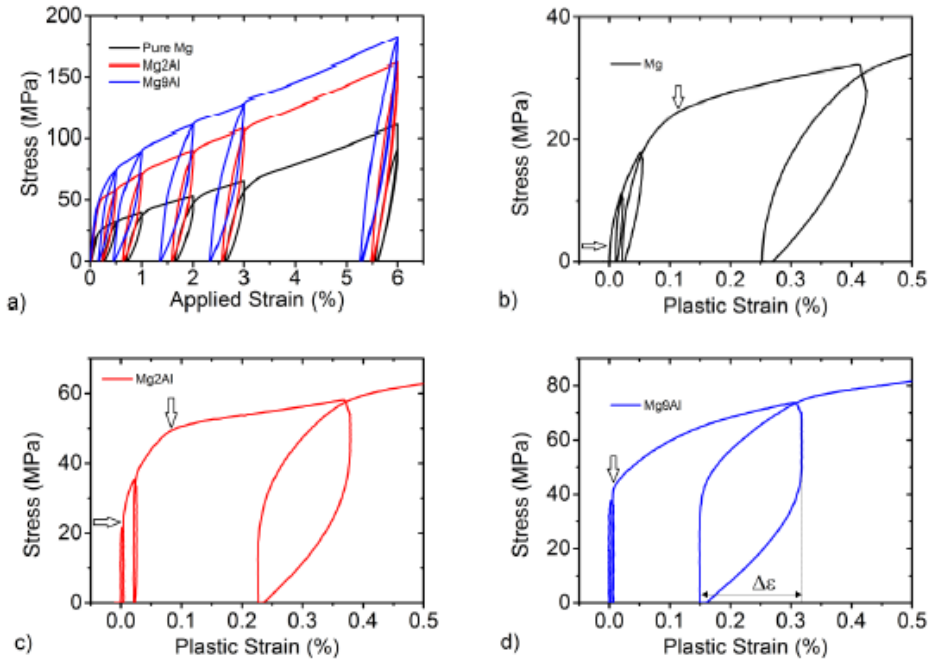

Fig. 1 Deformation curves during repetitive loading-unloading cycle of Mg-Al alloys. The onsets of the microplasticity and macroplasticity are indicated by the horizontal and vertical arrows, respectively.

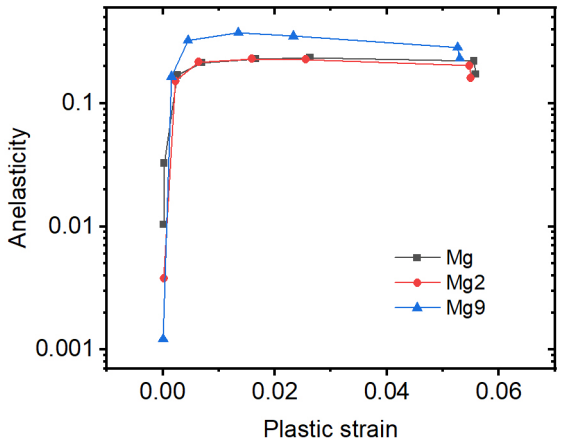

Fig. 2 Dependence of the anelasticity on the applied strain

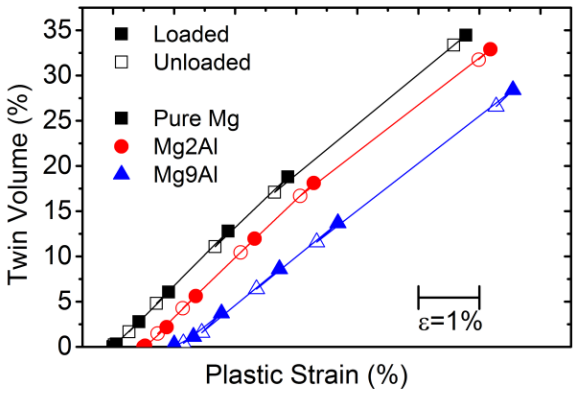

Fig. 3 TVF during the loading and unloading of the samples

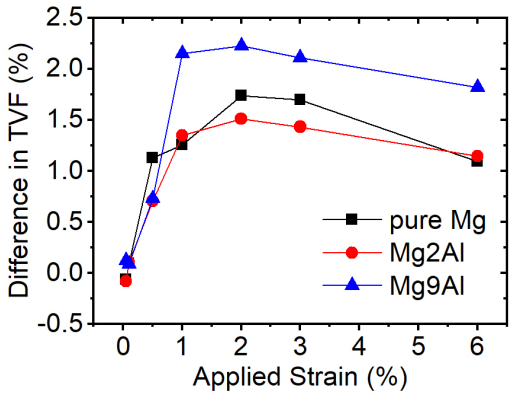

Fig. 4 Dependence of the twinned volume changes on the applied strain

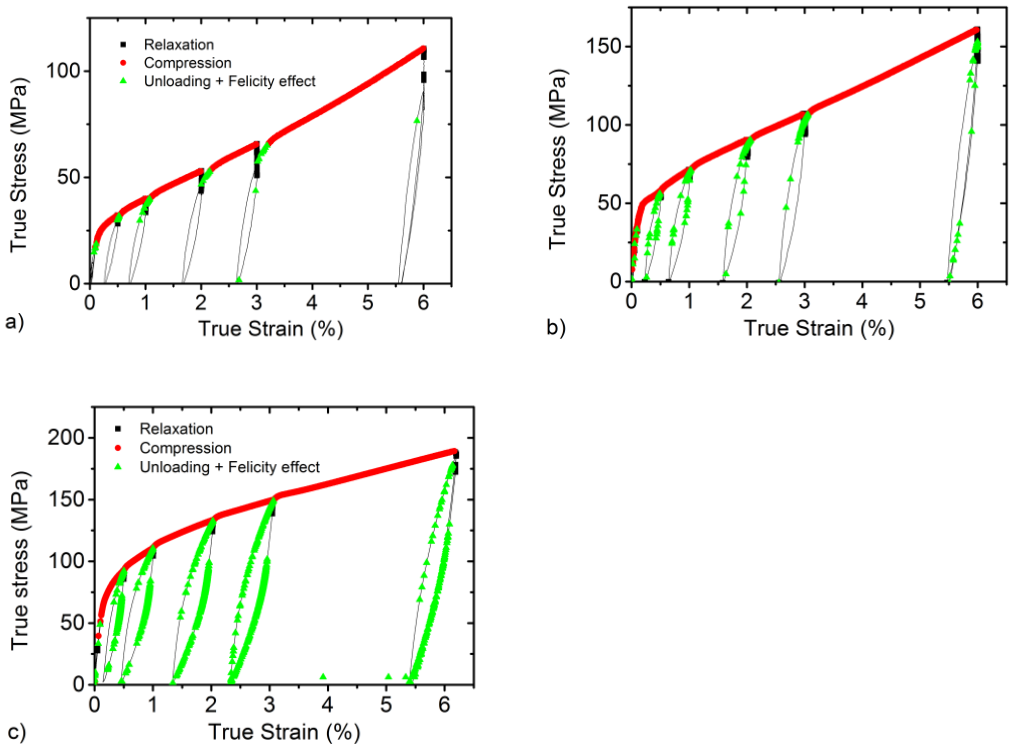

Fig. 5 AE events during the loading and unloading a) pure Mg, b) Mg2Al, c) Mg9Al

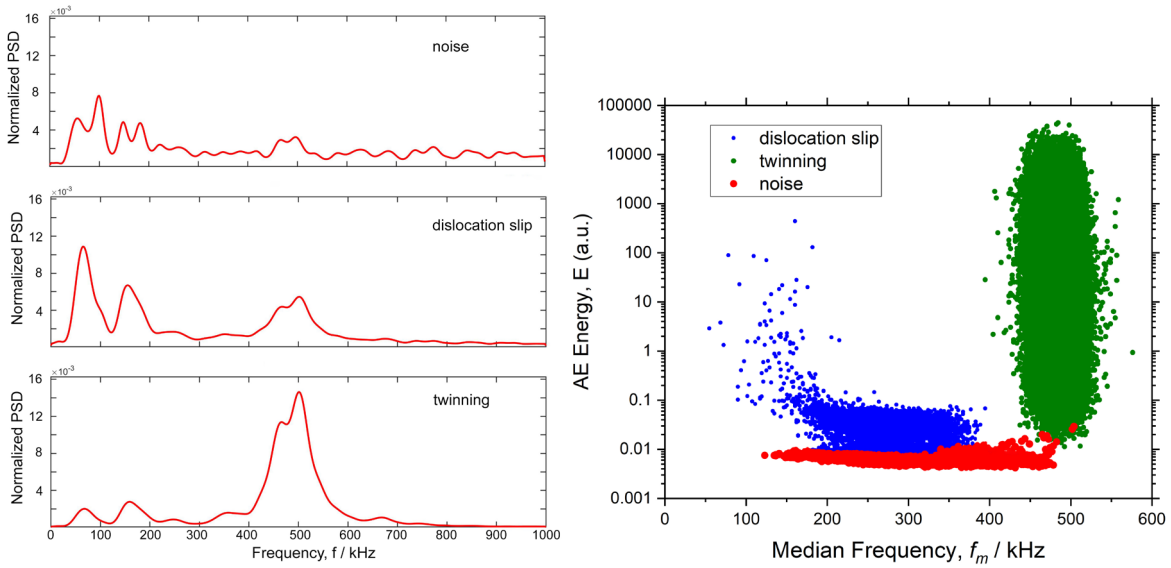

a) *b)*

Fig. 6 Normalized PSDs (a) and energy –mean frequency cross-plot (b) for the AE clusters identified by ASK analysis

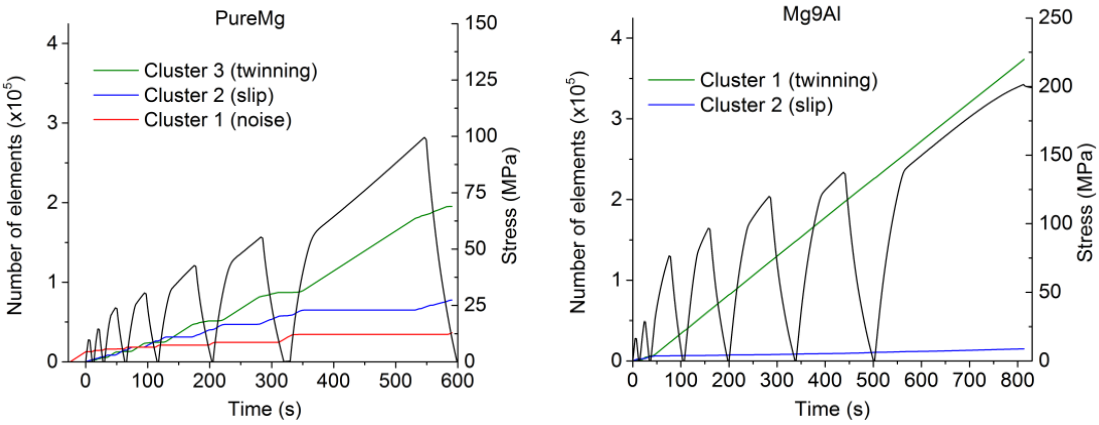

Fig. 7 ASK analysis of AE signal for a) pure Mg and b) Mg9Al sample

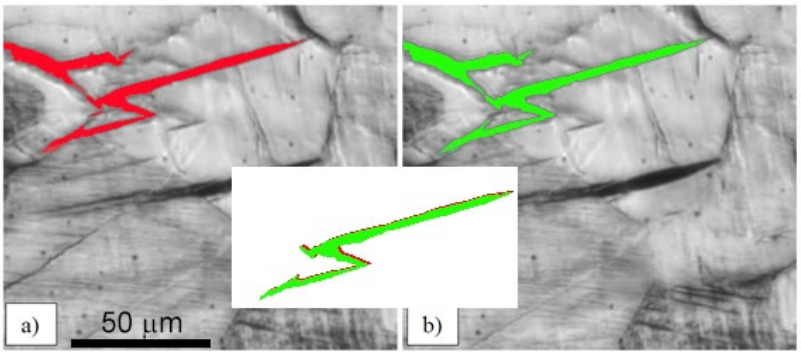

Fig. 8 High-speed camera observation: microstructure of pure Mg after a) loading up to 50 MPa and b) unloading up to 0 MPa. In the white rectangle the areas of highlighted twins on a and b are compared

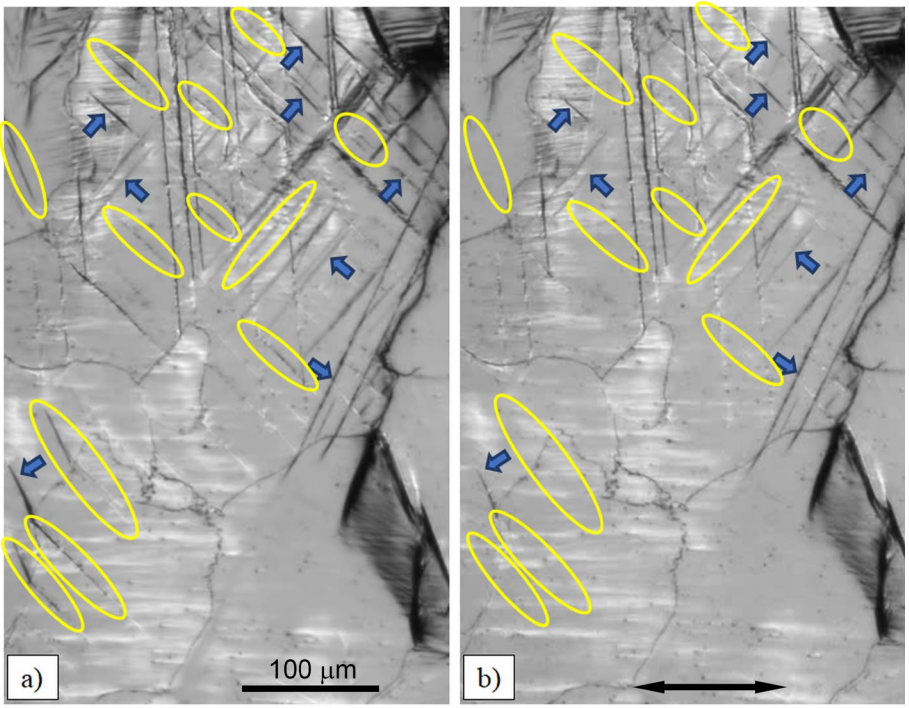

Fig. 9 High-speed camera observation: microstructure of the Mg9Al sample after a) loading up to 125 MPa and b) unloading up to 0 MPa. Shrinkage of twins is marked by arrows and complete detwinning - by circles. An arrow indicates the loading axis.

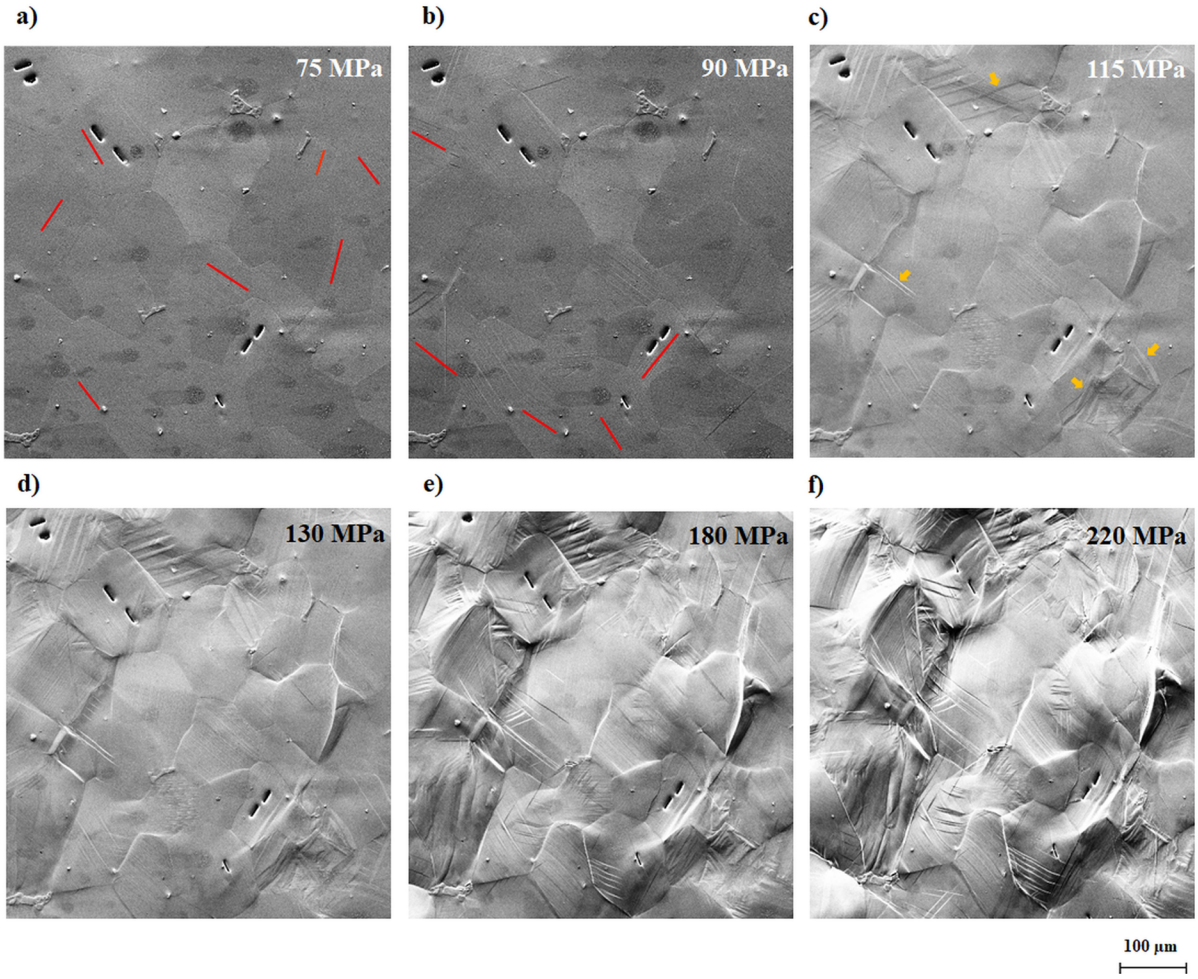

Fig. 10 In-situ SEM imaging: microstructure of the Mg9Al alloy after loading up to a) 75 MPa, b) 90 MPa, c) 115 MPa, d) 130 MPa, e) 180 MPa, f) 220 MPa, while each step of loading was followed by unloading up to 2 MPa. Red lines highlights traces of basal dislocation in grains, orange arrows – newly nucleated twins

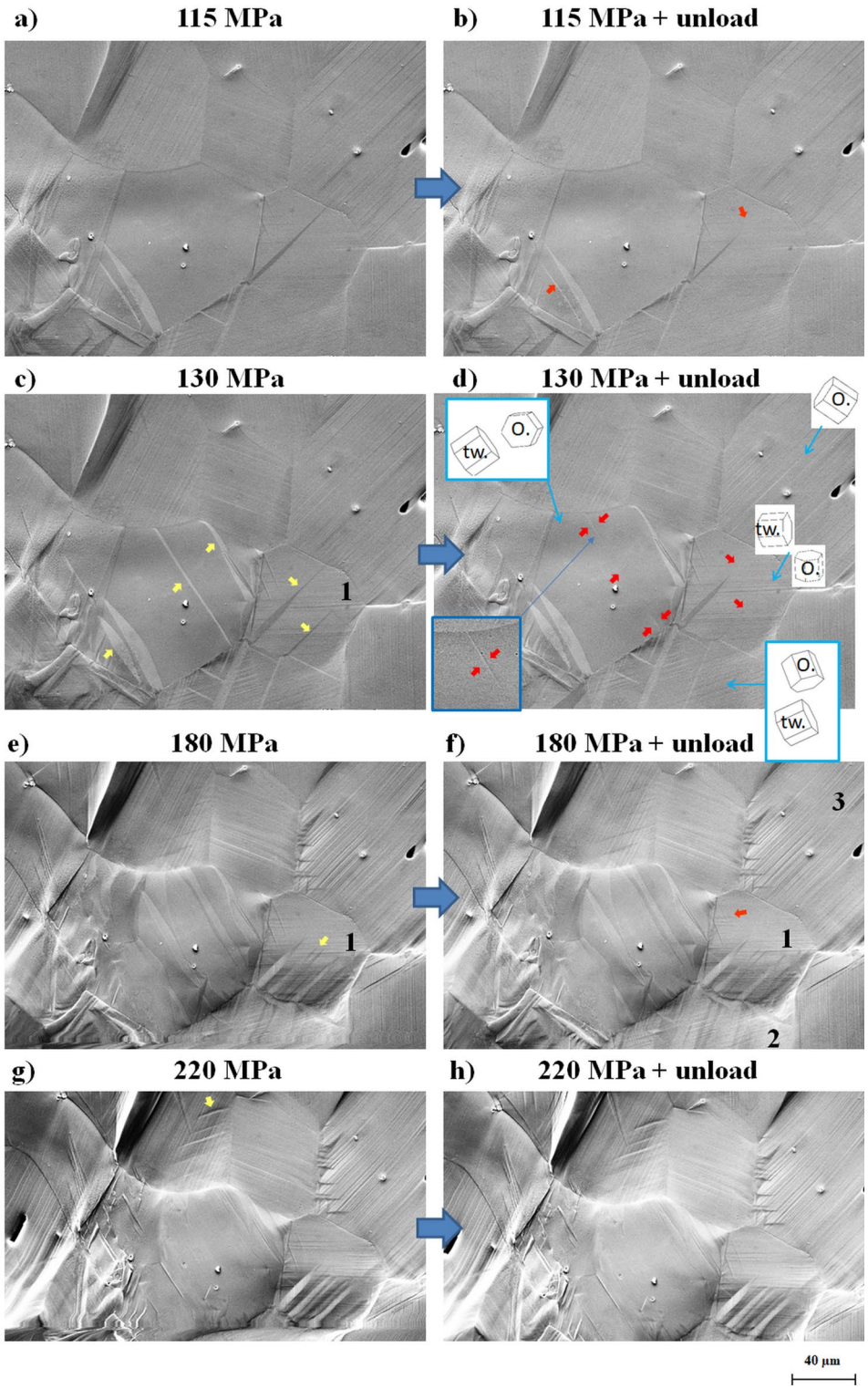

Fig. 11 In-situ SEM imaging: microstructure of the Mg9Al sample after (re)loading and unloading at each step of cyclic loading. Newly created twins and twin growth are highlighted by the yellow arrows, while detwinning is pointed out by the red one. O. - origin lattice orientation of the grain; tw. - twin orientation

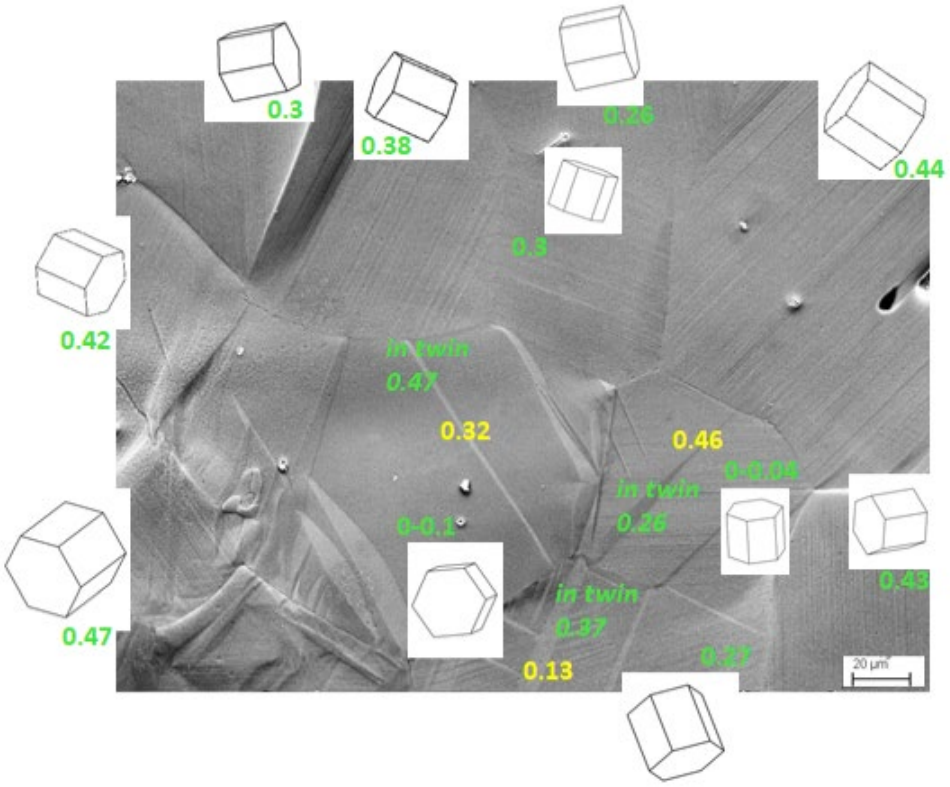

Fig. 12 Schmid factor calculation for the Mg9Al alloy: the values for basal slip are marked in green, the values for twins are marked in yellow

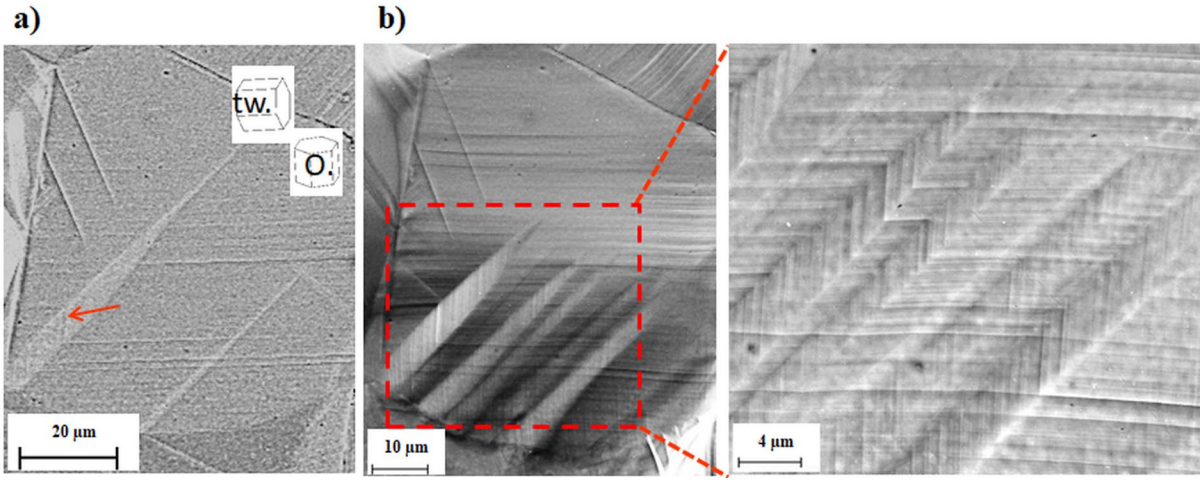

Fig. 13 In-situ SEM imaging: microstructure of the Mg9Al alloy after loading up to a) 130 MPa and b) 220 MPa and unloading up to 2 MPa. Traces of the dislocation lines correspond to basal slip

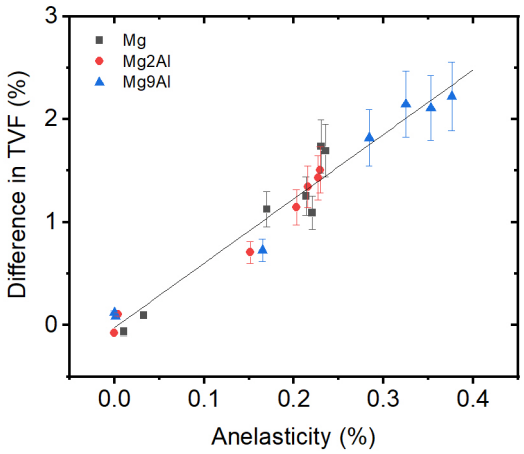

Fig. 14 Relation between the twinned volume fraction change during unloading and the anelastic strain

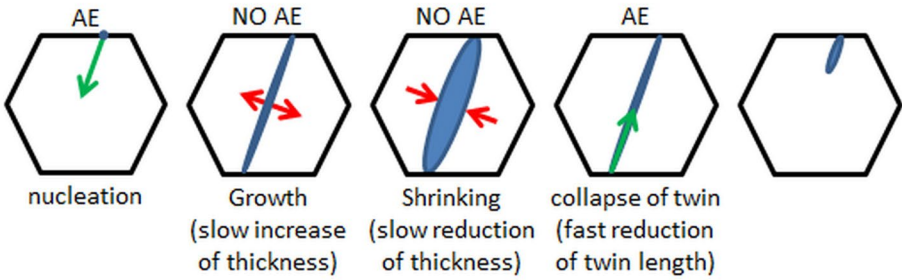

Fig. 15 Schematics of different stages of the twinning-detwinning process. Arrows indicate the direction of twin propagation: green color represents processes accompanied by detectable AE; red color corresponds to the processes which do not produce detectable AE